Reversible Watermarking Based on Invariant Image Classification and Dynamic Histogram Shifting

Gouenou Coatrieux, *Member, IEEE*, Wei Pan, Nora Cuppens-Boulahia, *Member, IEEE*, Frédéric Cuppens, *Member, IEEE*, and Christian Roux, *Fellow, IEEE*

***Abstract*—In this paper, we propose a new reversible watermarking scheme. One first contribution is a histogram shifting modulation which adaptively takes care of the local specificities of the image content. By applying it to the image prediction-errors and by considering their immediate neighborhood, the scheme we propose inserts data in textured areas where other methods fail to do so. Furthermore, our scheme makes use of a classification process for identifying parts of the image that can be watermarked with the most suited reversible modulation. This classification is based on a reference image derived from the image itself, a prediction of it, which has the property of being invariant to the watermark insertion. In that way, the watermark embedder and extractor remain synchronized for message extraction and image reconstruction. The experiments conducted so far, on some natural images and on medical images from different modalities, show that for capacities smaller than 0.4 bpp, our method can insert more data with lower distortion than any existing schemes. For the same capacity, we achieve a peak signal-to-noise ratio (PSNR) of about 1–2 dB greater than with the scheme of Hwang *et al.*, the most efficient approach actually.**

***Index Terms*—Medical image, reversible/lossless watermarking, signal classification.**

I. Introduction

FOR about ten years, several reversible watermarking schemes have been proposed for protecting images of sensitive content, like medical or military images, for which any modification may impact their interpretation [1]. These methods allow the user to restore exactly the original image from its watermarked version by removing the watermark. Thus it becomes possible to update the watermark content, as for example security attributes (e.g., one digital signature or some authenticity codes), at any time without adding new image distortions [2], [3] . However, if the reversibility property relaxes constraints of invisibility, it may also introduce discontinuity in data protection. In fact, the image is not protected once the watermark is removed. So, even though watermark removal is possible, its imperceptibility has to be guaranteed as most applications have a high interest in keeping the watermark in the image as long as possible, taking advantage of the continuous protection watermarking offers in the storage, transmission and also processing of the information [4]. This is the reason why, there is still a need for reversible techniques that introduce the lowest distortion possible with high embedding capacity.

Since the introduction of the concept of reversible watermarking in the Barton patent [5], several methods have been proposed. Among these solutions, most recent schemes use Expansion Embedding (EE) modulation [9], Histogram Shifting (HS) [7] modulation or, more recently, their combination. One of the main concern with these modulations is to avoid underflows and overflows. Indeed, with the addition of a watermark signal to the image, caution must be taken to avoid gray level value underflows (negative) and overflows (greater than $2^d - 1$ for a d bit depth image) in the watermarked image while minimizing at the same time image distortion. Basically, EE modulation introduced by Thodi *et al.* [9] is a generalization of Difference Expansion modulation proposed by Tian *et al.* [6] which expands the difference between two adjacent pixels by shifting to the left its binary representation, thus creating a new virtual least significant bit (LSB) that can be used for data insertion. Since then, EE has been applied in some transformed domains such as the wavelet domain [8], [9] or to prediction-errors. EE is usually associated with LSB substitution applied to "samples" that cannot be expanded due to the signal dynamic limits or in order to preserve the image quality. In [7], Ni *et al.* introduced the well-known Histogram Shifting (HS) modulation. HS adds gray values to some pixels in order to shift a range of classes of the image histogram and to create a 'gap' near the histogram maxima. Pixels which belong to the class of the histogram maxima ("*Carrier-class*") are then shifted to the gap or kept unchanged to encode one bit of the message '0' or '1'. Other pixels (the "noncarriers") are simply shifted. Instead of working in the spatial domain, several schemes apply HS to some transformed coefficients [10] or pixel prediction-errors [11], [12] , histograms of which are most of the time concentrated around one single class maxima located on zero. This maximizes HS capacity [10]–[12] and also simplifies the reidentification of the histogram classes of maximum cardinality at the extraction stage. In order to reduce the distortion while preserving the capacity, some preprocessing has been suggested in order to identify pixels, transformed coefficients or predic-

Manuscript received February 19, 2012; revised September 12, 2012; accepted September 22, 2012. Date of publication October 11, 2012; date of current version December 28, 2012. The work presented in this paper was supported in part by the ANR through the funding of the ANR SELKIS project. The associate editor coordinating the review of this manuscript and approving it for publication was Dr. Z. Jane Wang.

G. Coatrieux, W. Pan, and C. Roux are with the Institut Telecom; Telecom Bretagne; Unite INSERM 1101 Latim, Technopole Brest-Iroise, CS 83818, 29238 Brest Cedex 3, France (e-mail: gouenou.coatrieux@telecom-bretagne.eu; wei.pan@telecom-bretagne.eu; christian.roux@telecom-bretagne.eu).

N. Cuppens-Boulahia and F. Cuppens are with the Institut Telecom; Telecom Bretagne; UMR CNRS 3192 Labsticc, CS 17607, 35576 Cesson Sévigné Cedex, France (e-mail: nora.cuppens@telecom-bretagne.eu; frederic.cuppens@telecom-bretagne.eu).

Color versions of one or more of the figures in this paper are available online at http://ieeexplore.ieee.org.

Digital Object Identifier 10.1109/TIFS.2012.2224108

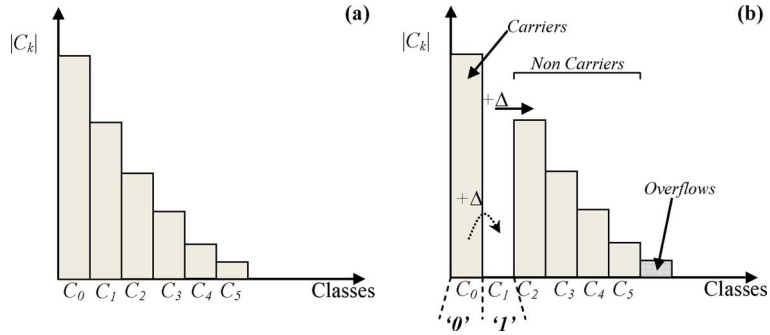

Fig. 1. Histogram shifting modulation. (a) Original histogram. (b) Histogram of the watermarked data.

tion-errors that do not belong to the histogram maxima classes ("*noncarrier classes*"). As we will see later, different schemes working with prediction-errors do not watermark pixels within a neighborhood of high variance [11]–[13]; indeed, these pixels belong to histogram classes that are shifted without message embedding. Recently, Hwang *et al.* [12] improved the approach of Sachnev *et al.*. They suggest defining the set of carrier-classes as the classes which minimize, for a given capacity, image distortion. However, their set of carrier-classes is uniquely defined for the whole image and the execution time of this approach is rather high.

In our view, none of the previous methods takes full advantage of the pixel neighborhood. We propose to adapt dynamically the carrier-classes by considering the local specificities of the image. We simply suggest using the local neighborhood of each prediction-error in order to determine the most adapted carrier-class for message insertion.

Another refinement we propose is based on the selection of the most locally adapted lossless modulation. Indeed, reversible modulations are more or less efficient depending on image content. This is especially the case for medical images where large black areas exist (i.e., the background area). In these regions, directly applying HS on pixels may be more efficient and of smaller complexity than applying it on prediction-errors. Because, the histogram maxima corresponds to the null gray value; capacity is maximized and underflows simply avoided by shifting pixel value to the right, i.e. by adding a positive gray value. When working on prediction-errors in these regions, the management of overflows/underflows is more difficult because the shift amplitude can be positive or negative. This is why we suggest considering the local content of the image in order to select the most locally adapted lossless modulation. This should allow us to optimize the compromise capacity/image distortion. The problem to solve is then how to synchronize the watermark embedder and extractor. Indeed, for message extraction, the extractor needs to know which modulation to use. The solution we propose is derived from one of our previous work [10] where an image classification process is exploited in order to identify the areas of the image that can be additively watermarked without introducing underflows/overflows. This classification process is conducted on a reference image derived from the image itself, a prediction of it, and it has the property of being invariant to the watermark insertion process. Thus, the watermark embedder and extractor remain synchronized because the extractor will retrieve the same reference image. Herein, we adapt this process to select the most locally appropriate watermarking modulation.

The rest of the paper is organized as follows. The main principles of our "Dynamic" Histogram Shifting modulation are introduced in Section II. Section III is devoted to our overall scheme and presents the way we merge classification and HS modulations. Section IV sums up the performance analysis of our scheme in terms of imperceptibility and capacity on different sets of medical images from different modalities as well as on some well-known natural test images like Lena. A comparison with the most efficient approaches [9]–[12] is also performed. Conclusions are provided in Section V.

II. Classical and Dynamic Histogram Shifting

A. Basic HS Modulation Principles

Originally introduced by Ni *et al.* in the spatial domain [7], the basic principle of Histogram Shifting modulation, illustrated in Fig. 1 in a general case, consists of shifting a range of the histogram with a fixed magnitude Δ, in order to create a 'gap' near the histogram maxima (C_1 in Fig. 1). Pixels, or more generally samples with values associated to the class of the histogram maxima (C_0 in Fig. 1(b)), are then shifted to the gap or kept unchanged to encode one bit of the message, i.e., '0' or '1'. As stated previously, we name samples that belong to this class as "*carriers*". Other samples, i.e., "*noncarriers*", are simply shifted. At the extraction stage, the extractor just has to interpret the message from the samples of the classes C_0 and C_1 and invert watermark distortions (i.e., shifting back shifted value). Obviously, in order to restore exactly the original data, the watermark extractor needs to be informed of the positions of samples that have been shifted out of the dynamic range ($[v_{\min}, v_{\max}]$ in Fig. 1(b)), samples we refer as overflows or underflows (Fig. 1(b) only illustrates "*overflows*"). This requires the embedding of an overhead and reduces the watermark capacity. Typically this overhead corresponds to a location map (a vector) whose components inform the extractor if samples of value $v_{\max}$ are original values or shifted values. In fact, considering the example in Fig. 1, the HS payload (C), i.e., the number of message bits embedded per sample of host data, is defined as:

$$C = |C_0| - (|C_{v_{\max}}| + |C_{v_{\max}-1}|) \tag{1}$$

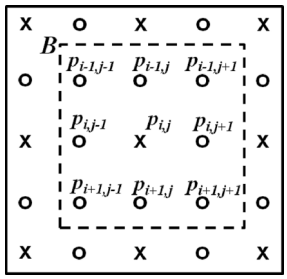

Fig. 2. Pixel neighborhood for prediction—in a 3×3 pixels block B, $p_{i,j}$ is estimated through its four nearest neighbors $p_{i-1,j}, p_{i,j+1}, p_{i+1,j}$, and $p_{i,j-1}$.

where C_0 is the class of carrier samples (see Fig. 1), $C_{v_{\max}}$ and $C_{v_{\max}-1}$ are classes associated to "overflows" and $|.|$ gives the class cardinality. Herein, the location map is a binary vector of $|C_{v_{\max}}| + |C_{v_{\max}-1}|$ bits long. One of its component indicates if a watermarked sample of value $v_{\max}$, is or is not a shifted sample. In that case, a host image can be HS watermarked if the capacity given by $|C_0|$ is greater than the overhead length, i.e., $|C_{v_{\max}}| + |C_{v_{\max}-1}|$. More generally, HS cannot be applied to data uniformly distributed. Conversely, the HS modulation will be efficient when histograms are concentrated around one single maxima. As an example, HS will provide good performances within black areas in medical images where the pixels have almost null gray values (these areas may occupy a large part of the image as shown in Fig. 5). However, images with such a histogram limited to one single maxima are not so common. Consequently, the achieved capacities remain limited. At the same time, the issue of histogram maxima retrieval by the watermark extractor may become more difficult to address. This is why the most recent works modulate wavelet subbands coefficients [9], [10] or the prediction-error of pixels, the distributions of which being most often Laplacian or Gaussian. In [9], Thodi *et al.* applied HS to the difference of two adjacent pixels for data embedding. In [10], we extended the Ni *et al.* scheme to Haar wavelet coefficients. In [11], Sachnev *et al.* propose to predict pixels through their four nearest neighbors and apply HS to the prediction-error. They achieve better performances than earlier existing schemes. In fact, it appears that the distribution of their prediction-error has a smaller variance than those of pixel differences or Haar wavelet coefficients. The choice of the wavelet transform or of the predictor will obviously impact the algorithm performance [14].

From here on, we work with the image prediction-error. Considering the pixel block in Fig. 2, the prediction-error $e_{i,j}$ of the pixel $p_{i,j}$ is given by $e_{i,j} = p_{i,j} - \hat{p}_{i,j}$, where $\hat{p}_{i,j}$ is the predicted value of $p_{i,j}$ derived as in [11], [12] from its four nearest neighbor pixels :

$$\hat{p}_{i,j} = \frac{(p_{i-1,j} + p_{i,j+1} + p_{i+1,j} + p_{i,j-1})}{4}. \qquad (2)$$

The prediction-error can thus be HS modulated as illustrated in Fig. 3(a). In that case, prediction-errors which do not belong to the carrier-class $C_c = [-\Delta, \Delta[$ are considered as "*noncarriers*" and are shifted of $+/-\Delta$ depending on their sign ($+\Delta$ if $e_{i,j} \geq 0$; $-\Delta$ if $e_{i,j} \leq 0$). Prediction-errors within the class $C_c = [-\Delta, \Delta[$, the "*carriers*", are used for embedding. $e_{i,j}$ is left unchanged to encode '0' or shifted to the range $[-2\Delta, -\Delta[$ or $[\Delta, 2\Delta[$, depending on its sign, to encode '1'. Notice that, even though message insertion is conducted in the prediction-error, it is the image pixels which are modulated. As a consequence, overflows and underflows appear in the spatial domain. It must be known, even though this is quite rare, that overflows/underflows may also appear in the prediction-error domain, for instance when the image is saturated by noise.

From this standpoint, different refinements have been proposed in order to optimize capacity and minimize distortion. Instead of simply shifting by Δ carrier prediction-errors, some authors apply EE modulation to them (see Section I). We do not have space to go into details, but this process results in adapting the shifting amplitude to the prediction-error value instead of shifting all of them by a constant Δ. The capacity is identical but distortion is minimized. Sachnev *et al.* [11] as well as Hwang *et al.* [12] and some others [14], [15] take advantage of this refinement. Our scheme does not, even though it can. Distortion can also be minimized by avoiding shifting noncarrier prediction-errors. As stated earlier, these prediction-errors belong to blocks of high variance, i.e., blocks where the predictor bias is high. Recently, Hwang *et al.* [12] extended the scheme of Sachnev *et al.* [11] by looking iteratively for the frontiers between the carrier-classes and noncarrier classes so as to minimize image distortion at a given capacity rate. By doing so, they achieve the best performance reported so far.

B. Dynamic Histogram Shifting

As stated above, prediction-errors that encode the message belong to the carrier-class $C_c = [-\Delta, \Delta[$, other prediction-errors are noncarriers. This predicate is static for the whole image and does not consider the local specificities of the image signal. Moreover, because prediction acts as a low-pass filter, most prediction-error carriers are located within smooth image regions. Highly textured regions contain noncarriers. The basic idea of our proposal is thus to gain carriers in such a region by adapting the carrier-class C_c depending on the local context of the pixel or of the prediction-error to be watermarked. We propose a Dynamic Histogram Shifting modulation to achieve this goal.

Let us consider the dashed pixel block B in Fig. 2. Let us also assume that we aim only at modulating the prediction-errors $e_{i,j}$ (or equivalently $p_{i,j}$) indicated by 'x' in Fig. 2, leaving intact their immediate neighborhood. Because of the local stationarity of the image signal we can assume without too much risk that contiguous prediction-errors have the same behavior. As a consequence, we suggest considering the prediction-error neighborhood so as to better define the location of C_c on the prediction-error dynamic.

Taking the eight neighbors of $p_{i,j}$: $\{p_{i-k,j-l}\}_{k,l=-1\ldots1}$, we can get their respective prediction-errors $e_{i-k,j-l}$. We propose then to define the carrier-class C_c as the histogram range to which the absolute values of prediction-errors $\{|e_{i-k,j-l}|\}_{k,l=-1..1,k,l\neq 0,0}$ belong (see Fig. 3(b)): $C_c = [-m_e - \Delta/2, -m_e + \Delta/2[\cup[m_e - \Delta/2, m_e + \Delta/2[$, where m_e is the mean-value of $\{|e_{i-k,j-l}|\}_{k,l=-1..1,k,l\neq 0,0}$. Our choice in using the absolute value instead of using the

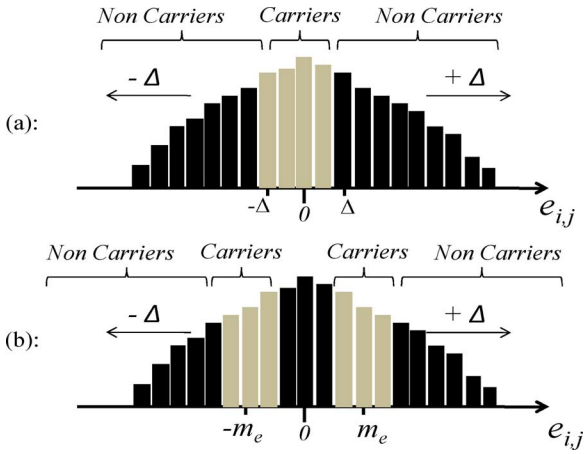

Fig. 3. HS modulation applied on predict errors: (a) classical modulation; (b) dynamical modulation.

prediction-error itself stands in the fact that contiguous prediction-errors are distributed around the zero value. Using their mean-value or a linear combination of them will result in predicting C_c centered on zero. Based on our approach, the reference class C_c is determined dynamically for each prediction-error of the image. In fact, it allows us to compensate the prediction-error in textured regions and consequently gives us the capability to insert data in such areas where other methods fail to do so.

It is important to notice that $p_{i,j}$ as well as all pixels identified by 'x' in Fig. 2 are modified after embedding. As a consequence, the prediction-error neighborhood of $p_{i,j}$ will also vary if it is computed based on (2). The solution we adopted to overcome this issue consists to use the predicted-value $\hat{p}_{i,j}$ instead of $p_{i,j}$ in (2). For example, the prediction-error $e_{i-1,j}$ is given by $e_{i-1,j} = p_{i-1,j} - \hat{p}_{i-1,j}$ with $\hat{p}_{i-1,j} = (\hat{p}_{i-2,j} + p_{i-1,j+1} + \hat{p}_{i,j} + p_{i-1,j-1})/4$. $p_{i-2,j}$ and $p_{i,j}$ are replaced by their predicted-value respectively. This means that the prediction-error neighborhood is not derived from the original image but from a copy of it where pixels for embedding are replaced by their predicted-values. An alternative to this strategy is to compute the prediction-error neighborhood using the diagonal pixel neighbors. However, this later approach appears to be less efficient.

As exposed, with our strategy, the location of C_c is computed independently of $e_{i,j,}$ (or equivalently of $p_{i,j,}$), and will be retrieved by the extractor: embedder and extractor remain synchronized without having to embed some extra-overhead. Nevertheless, our dynamic histogram shifting modulation requires performing the watermarking of the image in several passes. Herein, one quarter of the image pixels are watermarked at each pass in order to ensure that their prediction-error neighborhood remains unchanged (see Fig. 2). Going through the image into several passes in order to watermark all the pixels is not new. This is the case of most methods working with HS applied to pixel prediction-errors [11], [12].

The modulation we propose provides no advantage regarding overflows/underflows which still have to be managed. We come back to this issue in the next section where we proposed an original strategy for that purpose.

Let us also notice that, as for any HS modulations (see Section II-A), one can gain in performance by applying EE modulation on the prediction-error carriers instead of simply shifting them. For the same capacity, the distortion will be reduced. The scheme we present thereafter does not use EE. As a consequence, the performance we give in Section IV can be improved.

III. Proposed Scheme

As mentioned previously, our scheme relies on two main steps. The first one corresponds to an "invariant" classification process for the purpose of identifying different sets of image regions. These regions are then independently watermarked taking advantage of the most appropriate HS modulation. From here on, we decided distinguishing two regions where HS is directly applied to the pixels or applied dynamically to pixel prediction-errors respectively. We will refer the former modulation as PHS (for "*Pixel Histogram Shifting*") and the later as DPEHS (for "*Dynamic Prediction-Error Histogram Shifting*"). Our choice is based on our medical image data set, for which PHS may be more efficient and simple than the DPEHS in the image black background, while DPEHS will be better within regions where the signal is non-null and textured (e.g., the anatomical object). In the next section we introduce the basic concept of the invariance property of our classification process before detailing how it interacts with PHS and DPEHS. We also introduce some constraints we imposed on DPEHS in order to minimize image distortion and then present the overall procedure our scheme follows.

A. Invariant Image Classification

As said above, our classification process exploits a reference image $\hat{I}$ derived from the image I itself under the two following constraints : i) $\hat{I}$ remains unchanged after I has been watermarked into I_w, i.e., I and I_w have the same reference image; ii) $\hat{I}$ keeps the properties of an image signal so as to serve a classification process.

Even though PHS and DPEHS only modulate one pixel value within one block of the image (see Section II-B and Fig. 2), let us consider a more general framework where we watermark B^k, the k^{th} block of the image, by adding or subtracting a watermark pattern W, i.e., $B^k_w = B^k + / - W$. In our classification process, we associate the reference block $\hat{B}^k = \left[\hat{p}^k_{i,j}, \hat{p}^k_{i-N,j-N}, \ldots, \hat{p}^k_{i+N,j+N}\right]$ to $B^k = \left[p^k_{i,j}, p^k_{i-N,j-N}, \ldots, p^k_{i+N,j+N}\right]$. Considering linear algebra, the invariance constraint can be expressed as

$$\hat{B}^k = A \cdot B^k = A \cdot B^k_w = A \cdot \left(B^k \pm W\right) \tag{3}$$

where A is matrix of $(2N+1) \times (2N+1)$ coefficients for a block of $(2N+1) \times (2N+1)$ pixels. As defined, W is in the null space of A. At the same time, in order to ensure that $\hat{B}^k$ keeps the signal properties of an image, it can be designed as a predicted version or a low pass filtered version of B.

To exemplify this, let us consider again the 3×3 pixel block as illustrated in Fig. 2, and the watermark pattern $W = [1, 0, 0, 0, 0, 0, 0, 0, 0]$. In fact, W is added or subtracted

so as to apply PHS or DPEHS (see Sections II-A and II-B). In that case, the corresponding matrix A is given by:

$$\hat{B}^k = A \cdot B^k \tag{4}$$

$$\begin{bmatrix} \hat{p}^k_{i,j} \\ \hat{p}^k_{i-1,j-1} \\ \hat{p}^k_{i-1,j} \\ \hat{p}^k_{i-1,j+1} \\ \hat{p}^k_{i,j-1} \\ \hat{p}^k_{i,j+1} \\ \hat{p}^k_{i+1,j-1} \\ \hat{p}^k_{i+1,j} \\ \hat{p}^k_{i+1,j+1} \end{bmatrix} = \begin{bmatrix} 0 & 0 & \frac{1}{4} & 0 & \frac{1}{4} & \frac{1}{4} & 0 & \frac{1}{4} & 0 \\ 0 & 1 & 0 & 0 & 0 & 0 & 0 & 0 & 0 \\ 0 & 0 & 1 & 0 & 0 & 0 & 0 & 0 & 0 \\ 0 & 0 & 0 & 1 & 0 & 0 & 0 & 0 & 0 \\ 0 & 0 & 0 & 0 & 1 & 0 & 0 & 0 & 0 \\ 0 & 0 & 0 & 0 & 0 & 1 & 0 & 0 & 0 \\ 0 & 0 & 0 & 0 & 0 & 0 & 1 & 0 & 0 \\ 0 & 0 & 0 & 0 & 0 & 0 & 0 & 1 & 0 \\ 0 & 0 & 0 & 0 & 0 & 0 & 0 & 0 & 1 \end{bmatrix} \times \begin{bmatrix} p^k_{i,j} \\ p^k_{i-1,j-1} \\ p^k_{i-1,j} \\ p^k_{i-1,j+1} \\ p^k_{i,j-1} \\ p^k_{i,j+1} \\ p^k_{i+1,j-1} \\ p^k_{i+1,j} \\ p^k_{i+1,j+1} \end{bmatrix}. \tag{5}$$

The reference block of B^k corresponds then to $\hat{B}^k = \left[\hat{p}^k_{i,j}, p^k_{i-1,j-1}, \ldots, p^k_{i+1,j+1}\right]$ where $\hat{p}^k_{i,j}$ is a linear combination of $p^k_{i,j}$.

Once these constraints are fulfilled, the watermark extractor will retrieve exactly $\hat{I}$. Beyond, this allows us to characterize each block of the image by some simple measures extracted from its block of reference (e.g., maximum and minimum values, mean or standard deviation and so on). Such a block characterization is the basis of our classification process.

To illustrate this purpose, let us consider the first classification process whose objective for medical images is to discriminate regions that will be PHS or DPEHS watermarked. As stated, this corresponds merely distinguishing the black background of the image from the anatomical object. Let us continue also with the application matrix A in (5). In order to decide if one block B^k belongs to the background or not, one can simply characterizes B^k by its value $\hat{p}_{i,j}$ (issued from $\hat{B}^k$) and compare it to a threshold so as to take a decision. In our implementation, based on the fact that PHS and DPEHS are parameterized by a shift of magnitude Δ, we fixed this threshold equal to Δ, i.e., if $\hat{p}_{i,j} < \Delta$ then B^k belongs to the PHS region otherwise to the DPEHS region. From here on, we will also consider as part of the image background, blocks satisfying $\hat{p}_{i,j} > (2^d - 1) - \Delta$ (for a d bit depth image). The reason is because the medical image background sometimes contains saturated pixels corresponding to some annotations or markers that indicate, for example, the image acquisition orientation (e.g., right or left).

From that standpoint, we can distinguish different parts of the image and the extractor will be able to retrieve them easily if it knows A. Our scheme uses this approach not only for identifying image regions where to apply PHS or DPEHS but also for managing underflows and overflows, *i.e.* we do not have to watermark some extra-overhead data. We come back to this issue in the next section.

Notice also that the structure of the watermark pattern W can be made more complex. In fact, it depends on the insertion modulation. In [10], we carried out the embedding in the Haar wavelet transform of 2×2 pixel blocks considering a pattern W such as $\mathrm{W} = [1, -1, -1, 1]$.

B. Management of Underflows/Overflows

For sake of simplicity, let us consider one quarter of the image pixels for message embedding, i.e., the pixels indicated by 'x' in Fig. 2. Let us also consider a specific run into the image and note p^k the k^{th} pixel considered for embedding. Each pixel p^k can be framed by a block B^k of 3×3 pixels – see dashed block in Fig. 2 – to which is associated a reference block $\hat{B}^k = \left[\hat{p}^k_{i,j}, p^k_{i-1,j-1}, \ldots, p^k_{i+1,j+1}\right]$ computed using the matrix A in (5) ($\hat{p}^k_{i,j}$ is a linear prediction of $p^k_{i,j}$). $p^k_{i,j}$ will be PHS or DPEHS modulated. This can be viewed as the addition or subtraction of watermark pattern W to the block B^k, where $W = [1, 0, 0, 0, 0, 0, 0, 0, 0]$ (see above). As a consequence, despite the fact there is a block overlap, reference blocks remain invariant to the insertion process.

1) PHS Underflows/Overflows: According to the previous classification, PHS is applied to a pixel $p^k_{i,j}$ if its predicted-value falls in the range identified by $\hat{p}^k_{i,j} < \Delta$ (*low-part*) and $\hat{p}^k_{i,j} > (2^d - 1) - \Delta$ (*high-part*). Because in the low-part (resp. high-part), PHS shifts the pixels by adding (resp. subtracting) Δ gray values; there is no risk of underflow (resp. overflow). However, the risk an overflow (resp. underflow) occurs is not null. It happens when $\hat{p}^k_{i,j} < \Delta$ (resp. $\hat{p}^k_{i,j} > (2^d - 1) - \Delta$ while $p_{i,j} > (2^d - 1) - \Delta$ (resp. $p_{i,j} < \Delta$), it means when the pixel in the center of the block is completely different from its neighbors. Based on the fact that the image signal is usually highly correlated locally and that Δ corresponds to a few number of gray levels, these overflows (resp. underflows) are unlikely to happen. Even though such an overflow or underflow never occurred in all the experiments we conducted so far, our system handles this situation. It embeds along with the message an overhead constituted of two flags indicating an overflow and/or an underflow occurred followed by the necessary information for restoring the image pixels (see Section II-A).

2) DPEHS Underflows/Overflows: By definition (see Section II-B), DPEHS results in adding/subtracting Δ to $p^k_{i,j}$ (or adding/subtracting W to B^k) in order to modulate its prediction-error. Hence, some pixels may lead to an underflow/overflow if watermarked. To distinguish "*watermarkable*" pixels (or blocks), i.e., pixels that do not introduce overflow or underflow if modified, we propose a second classification process also based on the reference image $\hat{I}$, or more precisely on the reference block $\hat{B}^k$.

In order to build up this classification process we propose to characterize one pixel $p^k_{i,j}$ (or equivalently its framed block B^k) through some characteristics extracted from its reference block $\hat{B}^k$. The objective is to discriminate watermarkable pixels (or blocks) from the others with these characteristics. Herein, two characteristics are used. They are defined as $\hat{B}^k_{\min}$ and $\hat{B}^k_{\max}$

and correspond to the minimum and maximum values of $\hat{B}^k$ respectively. Then, considering in the image the N_o and N_u pixels (or equivalently blocks) that if watermarked by adding or subtracting Δ to $p^k_{i,j}$ (or by adding/subtracting W to B^k) lead to an overflow or and underflow respectively, we can identify two thresholds $T_{\min}$ and $T_{\max}$ such as

$$T_{\min} = \max_{n=1..Nu}(\hat{B}^n_{\min}); T_{\max} = \min_{m=1..No}(\hat{B}^m_{\max}). \quad (6)$$

A block B^k or its corresponding pixel $p^k_{i,j}$ is then considered as watermarkable if it satisfies the following constraints:

$$\hat{B}^k_{\min} > T_{\min} \text{ and } \hat{B}^k_{\max} < T_{\max} \quad (7)$$

otherwise, it is considered as nonwatermarkable and will not be modified. More clearly, we do not watermark pixels (or blocks) of same characteristics than those subject to overflows or underflows if watermarked. Notice that this classification process is done before DPEHS message insertion is conducted. Indeed we need to know which pixels are watermarkable.

Following the same strategy, conducted on some invariant characteristics, the extractor will reidentify nonwatermarkable pixels from the others. Nevertheless, in some cases, the extractor can identify threshold values $T^r_{\min}$ and $T^r_{\max}$ different from $T_{\min}$ and $T_{\max}$ computed at the embedding stage. In fact, some watermarked pixels (or blocks) may be identified by the extractor as subject to underflow or overflow changing at the same time the threshold values in a way such as $T^r_{\min} > T_{\min}$ and $T^r_{\max} < T_{\max}$. If this change occurs the extractor needs to be informed of the original values of $T_{\min}$ and $T_{\max}$ so as to retrieve all watermarked pixels and recover the original image perfectly. In our system, flag bits that indicate the change of $T_{\min}$ and $T_{\max}$ as well as their original values are embedded along with the message and a two step insertion process is used. During the first step, $T_{\min}$ and $T_{\max}$ and a part of the message is embedded considering the values of $T^r_{\min}$ and $T^r_{\max}$ the decoder will find. The remaining portion of the message is embedded by modifying the last watermarkable pixels. On the recipient side, the extractor will extract the first part of the message based on $T^r_{\min}$ and $T^r_{\max}$. It will get access to the rest of the information after a second reading step.

The way we manage threshold changes is based on the fact the embedder knows exactly what the extractor will see applying the same strategy. Thus, after having watermarked a pixel, the embedder checks if this one will be subject to an overflow or underflow from the extractor point of view and if it changes the threshold values. Most of the time, the change of $T_{\min}$ or $T_{\max}$ into $T^r_{\min}$ or $T^r_{\max}$ respectively is due to one noncarrier pixel (i.e., one pixel associated to one noncarrier prediction-error). The embedder can easily identify such a pixel as it can only be modified in one way (adding or subtracting Δ – see Section II-B). Then, informed by a flag bit the embedder has inserted along with the message, the extractor knows that $T^r_{\min}$ and/or $T^r_{\max}$ differ from $T_{\min}$ and/or $T_{\max}$ respectively and it has some other blocks to read and restore. Nevertheless, for some images, the change can occur on a carrier prediction-error. This situation is more difficult to handle as the pixel modification depends on the bit value of the message to be embedded (see Section II-A). More clearly, depending if the bit value to embed is equal to '0' or '1', the threshold change may occur or not. To overcome this problem, we decided to embed in the pixel the bit value that causes the threshold change and to inform the extractor of that situation by inserting another flag bit set to 1 along with the message. At the decoding stage, the extractor knows that the change occurs on a carrier prediction-error and will not consider the embedded bit as part of the message. It will restore such a pixel according to this rule.

(a) (b)

Fig. 4. Natural test images, gray-scale images of 512 × 512 pixels: (a) Lena; (b) Baboon.

To summarize, the DPEHS overhead contains: four flag bits indicating if $T^r_{\min} \neq T_{\min}$ and $T^r_{\max} \neq T_{\max}$ and if the change occurs or not on carrier prediction-error. If necessary, $T_{\min}$ or/and $T_{\max}$ are also encoded in the overhead. Thus, our overhead is of very small size. This contributes to the better performance of our system in terms of capacity.

C. DPEHS and Distortion Minimization

In order to minimize the distortion, we also propose two other refinements or constraints to be satisfied by DPEHS watermarkable pixels (or blocks). Firstly, like Sachnev *et al.* and some others [11], [13], we do not watermark blocks or pixels of too large estimator biases. These pixels belong to highly textured blocks. They can be identified through the standard deviation from their block of reference. Thus $p^k_{i,j}$ (or B^k) is watermarkable if it also satisfies

$$\hat{B}^k_{std} < T_{std} \quad (8)$$

where $\hat{B}^k_{std}$ is the standard deviation of $\hat{B}^k$ and T_{std} is a threshold we define in this study as the standard deviation mean of all reference blocks. Contrary to Sachnev *et al.* [11] and others [13], our extractor will retrieve T_{std}, computing it by itself, and will achieve the same classification.

Along the same line, we do not DPEHS watermark blocks which carrier-class C_c cannot be identified accurately. These blocks are characterized by a prediction-error neighborhood of high standard deviation e^k_{std}. Thus $p^k_{i,j}$ is modified if

$$e^k_{std} < T_e \quad (9)$$

where T_e corresponds to the mean of $\{e^k_{std}\}$ over the whole image. It is important to notice that, the prediction-error neighborhood considered here is the same as in Section II-B. This one is computed replacing in (2) the value of pixels considered for embedding by their predicted values.

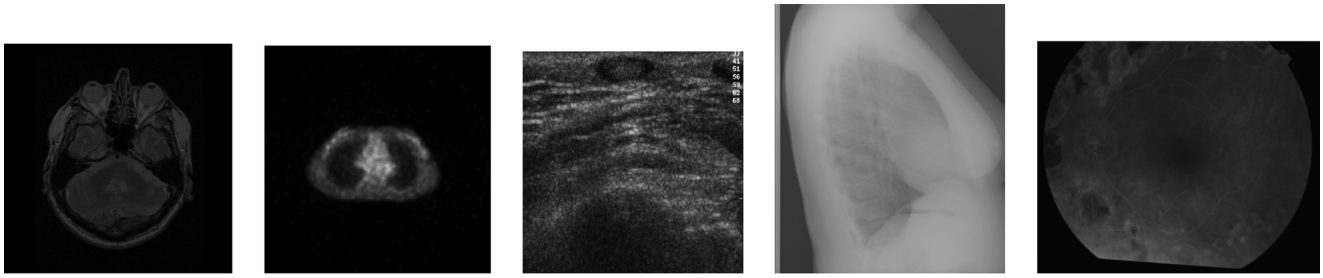

(a) (b) (c) (d) (e)

Fig. 5. Image samples from our different medical image test sets: (a) 12-bit encoded MRI axial slice of the head of 256 × 256 pixels; (b) 16-bit encoded PET image of 144 × 144 pixels; (c) 8-bit encoded ultrasound image of 480 × 592 pixels,; (d) 12-bit encoded X-ray image of 2446 × 2010 pixels; (e) 8-bit encoded retina image of 1008 × 1280 pixels.

D. Overall Scheme

To sum up, our algorithm runs through the image between one and four times. Each embedding pass is conducted independently from the other on one quarter of the image pixels considering the following procedure:

1. Considering a specific run into the image, possibly based on a secret key, pixels are classified into PHS region or DPEHS region. For that purpose, pixels are estimated using (2).
2. One part of the message is embedded in the PHS region along with some overhead in case of overflows/underflows (see Section III-B).
3. The rest of the message is embedded into the pixels of the DEPHS region according the following steps:
   a. Step 1: as depicted in Section III-B, the classification thresholds $T_{\min}$ and $T_{\max}$ are computed in order to discriminate watermarkable pixels from the others. At the same time the embedder verifies if the extractor will find or not the same thresholds. For that purpose, the watermark $W = [1,0,0,0,0,0,0,0,0]$ is considered while each pixel is associated with a reference block of 3×3 pixels using the matrix A (see Section III-B). Pixel prediction-errors as well as prediction-error neighborhoods are also computed (see Section II-B). This information is necessary to the embedder so as to manage threshold changes (i.e., to know if the changes occur on a carrier prediction-error or a noncarrier prediction-error). At the end of this process, the embedder builds the message overhead (flags concatenated with the values of $\mathrm{T}_{\min}$ and $\mathrm{T}_{\max}$ in case $\mathrm{T}^r_{\min} \neq \mathrm{T}_{\min}$ and $\mathrm{T}^r_{\max} \neq \mathrm{T}_{\max}$) and computes the thresholds T_{std} and T_e (see Section III-C).
   b. Step 2: message embedding is conducted in one or two stages depending if $T^r_{\min} \neq T_{\min}$ and $T^r_{\max} \neq T_{\max}$ and on the value of T_{std} and T_e.

At the extraction stage, in the case the matrix A is predefined, the only parameter the extractor needs to know is the histogram shifting amplitude Δ which parameterizes PHS and DPEHS as well as the classification processes (see Sections III-A and III-B). Notice that in this scheme, the value of Δ is fixed by the user. Message extraction is conducted independently in each region and pass. For the DPEHS message, the extractor will retrieve by itself the values of $T_{\min}$, $T_{\max}$, T_{std} and T_e and will apply or not a two-stage message extraction process (see Section III-B).

IV. Experiments

A. Image Database and Measures of Performance

The previous watermarking scheme has been tested and compared with some recent methods [9]–[12]. All have been applied to several natural gray-scale images (like Lena and Baboon (see Fig. 4), used as reference in the literature), and different series of medical images issued from five distinct modalities. These image sets, illustrated in Fig. 5, contain respectively:

- three 12 bit encoded Magnetic Resonance Image (MRI) volumes of 79, 80 and 99 axial slices of 256 × 256 pixels respectively;
- three 16 bit encoded Positron Emission Tomography (PET) volumes of 234, 213 and 212 axial slices of 144 × 144 pixels respectively;
- three sequences of 8 bit encoded Ultrasound (US) images. The first sequence contains 14 images of 480 × 592 pixels, and the two others 9 and 30 images of 480 × 472 pixels respectively;
- forty two 12 bit encoded X-ray images of 2446 × 2010 pixels, and;
- thirty 8 bit encoded retina images of 1008 × 1280 pixels.

To objectively quantify achieved performance, different criteria have been considered:

— the capacity rate C expressed in *bpp* (bit of message per pixel of image);

— and, the Peak Signal to Noise Ratio (*PSNR*) so as to measure the distortion between an image I and its watermarked version I_w

$$PSNR = 10\log_{10}\left(\frac{NM\left(2^d-1\right)^2}{\sum\limits_{i,j=1,1}^{N,M}\left(I\left(i,j\right)-I_w\left(i,j\right)\right)^2}\right) \quad (10)$$

where d corresponds to the image depth and N and M to the image dimensions.

In the following experiments, the embedded message is a binary sequence randomly generated according to a uniform distribution.

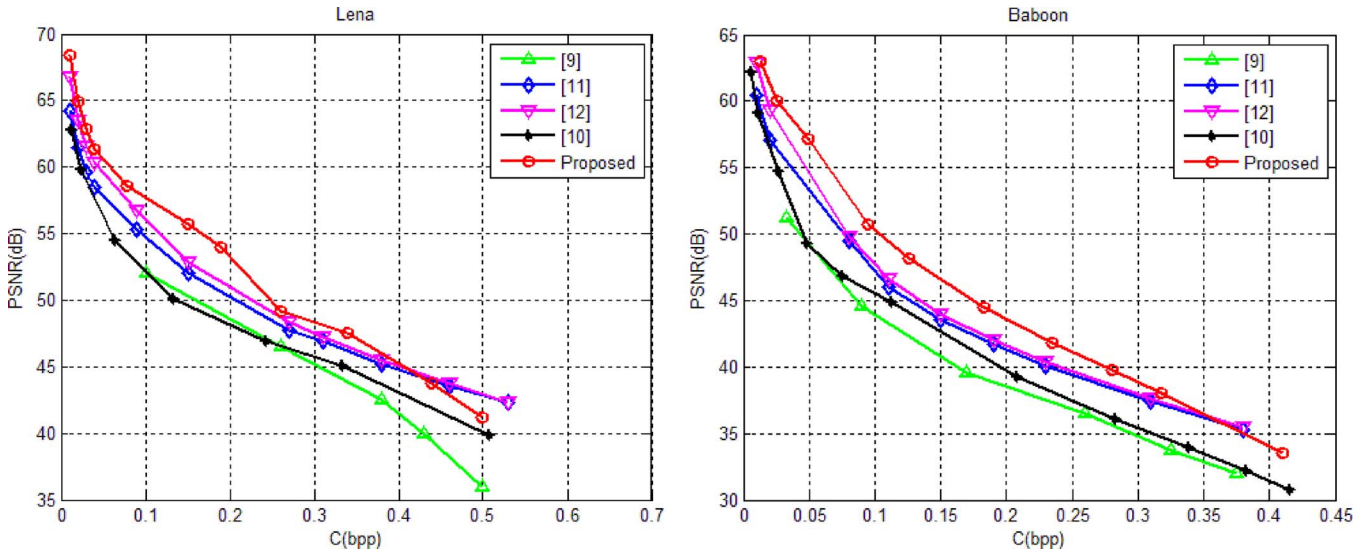

Fig. 6. Embedding capacity (C) versus image distortion ($PSNR$) of our approach in comparison with the reversible schemes [9]–[12]. The test set is constituted of gray-scale image Lena and Baboon.

TABLE I
COMPARISON ASSESSMENT IN TERMS OF CAPACITY AND DISTORTION FOR OUR APPROACH AND THOSE PROPOSED BY: SACHNEV [11], HWANG [12]. THE TEST SET IS CONSTITUTED OF GRAY-SCALE IMAGE LENA, BABOON

$\Delta = 1$		use of ¼ of the image I		use of ½ of the image I		use of the whole image I	
		C	PSNR	C	PSNR	C	PSNR
Lena	[11]	0.02	61.42	0.04	58.51	0.09	55.29
	[12]	0.03	61.54	0.08	56.78	0.11	54.58
	Proposed	0.04	61.375	0.078	58.545	0.15	55.72
Baboon	[11]	0.005	63.66	0.01	60.46	0.02	57.11
	12]	0.01	62.92	0.01	60.80	0.03	56.97
	Proposed	0.0127	63.026	0.025	60.077	0.049	57.167

B. Experimental Results

Results are given in Tables I–III and in Fig. 6 in terms of capacity and image distortion depending on: the pixel shifting magnitude Δ (see Section II); and the number of times our algorithm goes through the image (between 1 and 4 times, see previous section).

Results for natural images are given in Table I and Fig. 6, where we compare our technique with the four other schemes proposed in [9]–[12]. Presented curves have been obtained making varying Δ and the number of embedding passes progressively. Notice that the method of Hwang *et al.* [12], derived from the scheme of Sachnev *et al.* [11], is actually the best algorithm reported today. As can be seen from Fig. 6, our method provides a better capacity/distortion compromise than any of these methods [9]–[12] for low and medium capacities (i.e., capacities smaller than 0.4 bpp). For example, for a capacity of 0.15 *bpp*, our approach provides a *PSNR* of 55.72 dB for Lena, a PSNR value about 2.8 dB higher than [12]. From Table I which sums up results obtained for high *PSNR* values, most of the time our method allows twice the capacities obtained by Sachnev *et al.* [11] and about 1.3 the capacities of Hwang *et al.* [12]. Most of the gain our scheme is issued from our dynamic histogram shifting modulation. This can be seen from the Lena image. Indeed, because this latter does not contain black areas, only our DPEHS modulation applies for message embedding. It is quite the same for Baboon. Nevertheless, for a capacity rate greater than 0.4 bpp, our scheme is less efficient than [11] and [12] or than methods presented in [16], [17] which are even better.

For medical images, the results are somewhat equivalent to those obtained for natural images. Compared to [9]–[12], our approach better preserves the image quality for the same capacity rate, as indicated in Table II. If we go into detail (see Table III), our gain is about 1.5–2 *dB* and 4–5 *dB* of *PNSR* compared to [12] and [11] respectively. However, our approach has somewhat equivalent performance for PET images. Such a similarity can be explained by the fact that the strategies followed by [11] and [12] have close performance to that of PHS in the image black background which herein occupies a large part of the image (see the sample depicted in Fig. 5(b)). Again and like for natural images, the gain of our scheme is issued from the better behavior of our DPEHS modulation within areas where the signal exists (herein the anatomical object). Nevertheless, whatever the medical image modality, our method proposes the best compromise in terms of image quality preservation for low and medium capacities.

TABLE II
COMPARISON ASSESSMENT IN TERMS OF CAPACITY AND DISTORTION OF OUR APPROACH AND THOSE PROPOSED BY THODI [9], PAN [10], SACHNEV [11], AND HWANG [12]. RESULTS ARE GIVEN IN AVERAGE PER IMAGE WITH THEIR STANDARD DEVIATION BETWEEN PARENTHESES

	MRI		PET		US	
	C (bpp)	*PSNR (dB)*	*C (bpp)*	*PSNR (dB)*	*C (bpp)*	*PSNR (dB)*
[9]	0.0214 (0.004)	72.41 (0.168)	0.13 (0.025)	97.27 (0.30)	0.22 (0.09)	48.44 (0.769)
[10]	0.006 (0.004)	78.62 (0.82)	0.029 (0.02)	101.31 (1.06)	0.2 (0.02)	51.1 (0.34)
[11]	0.25 (0.005)	74.81 (0.15)	0.17 (0.023)	105.18 (0.5)	0.15 (0.05)	52.75 (0.55)
[12]	0.25 (0.005)	78.00 (0.25)	0.17 (0.02)	105 (0.5)	0.15 (0.05)	55.00 (0.5)
Proposed	0.25 (0.005)	79.06 (0.5)	0.17 (0.03)	105.35 (0.5)	0.16 (0.03)	57.067 (0.4)

TABLE III
CAPACITY AND DISTORTION MEASUREMENTS FOR OUR APPROACH AND FOR THE REVERSIBLE SCHEMES OF SACHNEV [11], HWANG [12] IN APPLICATION TO MRI, PET, US, RETINA, X-RAY IMAGES. INDICATED PERFORMANCE ARE GIVEN IN AVERAGE PER IMAGE WITH THEIR STANDARD DEVIATION BETWEEN PARENTHESES

$\Delta = 1$		use of ¼ of the image I		use of ½ of the image I		use of the whole image I	
		C(bpp)	*PSNR*	*C(bpp)*	*PSNR*	*C(bpp)*	*PSNR*
MRI	Proposed	0.064 (0.002)	84.99 (0.4)	0.13 (0.004)	81.94 (0.4)	0.25 (0.005)	79.06 (0.5)
	[12]	0.066 (0.002)	83.16 (0.35)	0.13 (0.0025)	80.11 (0.3)	0.25 (0.005)	77.16 (0.25)
	[11]	0.066 (0.0015)	80.84 (0.3)	0.13 (0.003)	77.79 (0.25)	0.25 (0.005)	74.81 (0.15)
PET	Proposed	0.088 (0.01)	108.16 (0.4)	0.17 (0.03)	105.35 (0.5)	0.32 (0.02)	102.58 (0.5)
	[12]	0.091 (0.01)	107.82 (0.5)	0.17 (0.02)	104.98 (0.5)	0.35 (0.03)	102.22 (0.5)
	[11]	0.088 (0.01)	107.85 (0.5)	0.17 (0.023)	105.18 (0.5)	0.35 (0.02)	102.16 (0.5)
US	Proposed	0.043 (0.025)	62.55 (0.3)	0.084 (0.03)	59.77 (0.52)	0.16 (0.03)	57.067 (0.4)
	[12]	0.038 (0.02)	59.41 (0.3)	0.079 (0.04)	56.35 (0.55)	0.16 (0.05)	53.85 (0.5)
	[11]	0.041 (0.02)	57.94 (0.4)	0.084 (0.05)	54.86 (0.57)	0.16 (0.05)	52.76 (0.55)
Retina	Proposed	0.06 (0.005)	62.19 (0.1)	0.11 (0.01)	59.40 (0.15)	0.21 (0.01)	56.47 (0.16)
	[12]	0.06 (0.004)	61.29 (0.2)	0.11 (0.01)	58.26 (0.2)	0.20 (0.01)	54.30 (0.15)
	[11]	0.06 (0.005)	58.74 (0.2)	0.10 (0.01)	56.75 (0.2)	0.22 (0.008)	53.75 (0.1)
X-ray	Proposed	0.007 (0.005)	86.98 (1.2)	0.014 (0.01)	83.98 (2)	0.028 (0.01)	81.00 (1.9)
	[12]	0.007 (0.005)	84.47 (1)	0.014 (0.01)	81.43 (1.5)	0.027 (0.008)	78.12 (1.5)
	[11]	0.007 (0.004)	82.42 (1)	0.014 (0.01)	79.37 (1.5)	0.027 (0.009)	76.46 (2.0)

V. CONCLUSION

In this paper, we have proposed a new reversible watermarking scheme which originality stands in identifying parts of the image that are watermarked using two distinct HS modulations: Pixel Histogram Shifting and Dynamic Prediction Error Histogram Shifting (DPEHS). The latter modulation is another original contribution of this work. By better taking into account the signal content specificities, our scheme offers a very good compromise in terms of capacity and image quality preservation for both medical and natural images. This scheme can still be improved. Indeed, like most recent schemes, our DPEHS can be combined with the expansion embedding (EE) modulation, as well as with a better pixel prediction. However, this method is fragile as any modifications will impact the watermark. Even though some solutions have already been proposed [18], [19], questions about watermark robustness are largely open. This is one of the upcoming challenges.

REFERENCES

[1] G. Coatrieux, C. Le Guillou, J.-M. Cauvin, and C. Roux, "Reversible watermarking for knowledge digest embedding and reliability control in medical images," *IEEE Trans. Inf. Technol. Biomed.*, vol. 13, no. 2, pp. 158–165, Mar. 2009.

[2] F. Bao, R. H. Deng, B. C. Ooi, and Y. Yang, "Tailored reversible watermarking schemes for authentication of electronic clinical atlas," *IEEE Trans. Inf. Technol. Biomed.*, vol. 9, no. 4, pp. 554–563, Dec. 2005.

[3] H. M. Chao, C. M. Hsu, and S. G. Miaou, "A data-hidding technique with authentication, integration, and confidentiality for electronic patient records," *IEEE Trans. Inf. Technol. Biomed.*, vol. 6, no. 1, pp. 46–53, Mar. 2002.

[4] G. Coatrieux, L. Lecornu, B. Sankur, and C. Roux, "A review of image watermarking applications in healthcare," in *Proc. IEEE EMBC Conf.*, New York, 2006, pp. 4691–4694.

[5] J. M. Barton, "Method and Apparatus for Embedding Authentication Information Within Digital Data," U.S. Patent 5 646 997, 1997.

[6] J. Tian, "Reversible data embedding using a difference expansion," *IEEE Trans. Circuits Syst. Video Technol.*, vol. 13, no. 8, pp. 890–896, Aug. 2003.

[7] Z. Ni, Y. Q. Shi, N. Ansari, and S. Wei, "Reversible data hiding," *IEEE Trans. Circuits Syst. Video Technol.*, vol. 16, no. 3, pp. 354–362, Mar. 2006.

[8] G. Xuan, Y. Q. Shi, C. Y. Yang, Y. Z. Zheng, D. K. Zou, and P. Q. Chai, "Lossless data hiding using integer wavelet transform and threshold embedding technique," in *Proc. Int. Conf. Multimedia and Expo*, 2005, pp. 1520–1523.
[9] D. M. Thodi and J. J. Rodriquez, "Expansion embedding techniques for reversible watermarking," *IEEE Trans. Image Process.*, vol. 16, no. 3, pp. 721–730, Mar. 2007.
[10] W. Pan, G. Coatrieux, N. Cuppens, F. Cuppens, and C. Roux, "An additive and lossless watermarking method based on invariant image approximation and Haar wavelet transform," in *Proc. IEEE EMBC Conf.*, Buenos Aires, Argentina, 2010, pp. 4740–4743.
[11] V. Sachnev, H. J. Kim, J. Nam, S. Suresh, and Y.-Q. Shi, "Reversible watermarking algorithm using sorting and prediction," *IEEE Trans. Circuit Syst. Video Technol.*, vol. 19, no. 7, pp. 989–999, Jul. 2009.
[12] H. J. Hwang, H. J. Kim, V. Sachnev, and S. H. Joo, "Reversible watermarking method using optimal histogram pair shifting based on prediction and sorting," *KSII, Trans. Internet Inform. Syst.*, vol. 4, no. 4, pp. 655–670, Aug. 2010.
[13] L. Kamstra and H. J. A. M. Heijmans, "Reversible data embedding into images using wavelet techniques and sorting," *IEEE Trans. Image Process.*, vol. 14, no. 12, pp. 2082–2090, Dec. 2005.
[14] L. Luo, Z. Chen, M. Chen, X. Zeng, and Z. Xiong, "Reversible image watermarking using interpolation technique," *IEEE Trans. Inf. Forensics Security*, vol. 5, no. 1, pp. 187–193, Mar. 2010.
[15] D. Coltuc, "Improved embedding for prediction-based reversible watermarking," *IEEE Trans. Inf. Forensics Security*, vol. 6, no. 3, pp. 873–882, Sep. 2011.
[16] C. C. Lin, W. L. Tai, and C. C. Chang, "Multilevel reversible data hiding based on histogram modification of difference images," *Pattern Recognit.*, vol. 41, pp. 3582–3591, 2008.
[17] C. H. Yang and M. H. Tsai, "Improving histogram-based reversible data hiding by interleaving predictions," *IET Image Process.*, vol. 4, no. 4, pp. 223–234, Aug. 2010.
[18] C. De Vleeschouwer, J.-F. Delaigle, and B. Macq, "Circular interpretation of bijective transformations in lossless watermarking for media asset management," *IEEE Trans. Multimedia*, vol. 5, no. 1, pp. 97–105, Mar. 2003.
[19] D. Coltuc and J.-M. Chassery, "Distortion-free robust watermarking: A case study," in *Proc. Security, Steganography, and Watermarking of Multimedia Contents IX*, San Jose, CA, 2007, p. 65051N-8.

Gouenou Coatrieux (M'06) received the Ph.D. degree in signal processing and telecommunication from the University of Rennes I, Rennes, France, in collaboration with the Institut Mines Telecom, Telecom Paris-Tech, Paris, France, in 2002. His Ph.D. focused on watermarking in medical imaging.

He is currently an Associate Professor in the Information and Image Processing Department, Institut Mines-Telecom, Telecom Bretagne, Brest, France, and his research is conducted in the Laboratoire de Traitement de l'Information Médicale, Unité INSERM U1101, Brest. His primary research interests include medical information system security, watermarking, electronic patient records, and healthcare knowledge management.

Dr. Coatrieux is an associate editor of the IEEE TRANSACTIONS ON INFORMATION TECHNOLOGY IN BIOMEDICINE and of the Elsevier journals *Digital Signal Processing* and *Biomedical Engineering and Research*. He is also a member of the IFMBE "Global Citizen Safety and Security Working Group" and has contributed to the Technical Committee of the Information Technology for Health (IT4H) of the IEEE Engineering in Medicine and Biology Society.

Wei Pan received the Ph.D. degree in signal processing and telecommunication from the University of Rennes I, Rennes, France, in collaboration with the Telecom Bretagne, Brest, France, in 2012, for research conducted in the Laboratoire de Traitement de l'Information Médicale, Unité INSERM U1101, Brest. His research interests are medical information system security, watermarking of medical imaging and electronic patient records, and access control policy.

Nora Cuppens-Boulahia (M'11) is an associate researcher at TELECOM Bretagne of Institut Mines-Telecom. She holds an engineering degree in computer science, the Ph.D. degree from ENSAE (National Higher School of Aeronautics and Space), and an HDR from University Rennes 1. Her research interests include formalization of security properties and policies, cryptographic protocol analysis, formal validation of security properties, and threat and reaction risk assessment. Her current research topics include *a posteriori* access and usage control and traceability, privacy preserving by query rewriting, data fragmentation, and security of web services. She has published more than 80 technical papers in refereed journals and conference proceedings. She has been member of several international program committees in information security system domain and the Program Committee Chair of SETOP 2008, SETOP 2009, SAR-SSI 2009, CRiSIS 2010, DPM 2011, SECOTS 2012, DBSEC 2012, PST 2012, and the cogeneral chair of ESORICS 2009. She is the French representative of IFIP TC11 "Information Security" and she is coresponsible for the information system security axis of the French learned society SEE.

Frédéric Cuppens (M'11) is a full professor at TELECOM Bretagne of Institut Mines-Telecom and coresponsible for SFIIS (security, reliability and integrity of systems' information), one of the CNRS LabSTICC teams. He holds an engineering degree in computer science, the Ph.D. degree and the HDR (Habilitation to supervise research). He has been working for more 20 years on various topics of computer security including definition of formal models of security policies, access control to network and information systems, intrusion detection, reaction and countermeasures, and formal techniques to refine security policies and prove security properties. He has published more than 150 technical papers in refereed journals and conference proceedings. He served on several conference program committees as member or as general chair. He was the Programme Committee Chair of several conferences including ESORICS 2000, IFIP SEC 2004, SAR-SSI 2006, SETOP 2008, CRISIS 2011, PST 2011, and DBSEC 2012.

Christian Roux (F'05) received the Aggregation degree in physics from the Ecole Normale Supérieure, Cachan, France, in 1978, and the Ph.D. degree from the Institut National Polytechnique, Grenoble, France, in 1980.

In 1982, he joined the Institut Mines-Telecom, Telecom Bretagne, Brest, France, where he became an Associate Professor in 1987 and has been a Professor since 1987. He was a Visiting Professor with the Medical Image Processing Group, Department of Radiology, University of Pennsylvania (1992–1993), and a Distinguished International Research Fellow with the Department of Electrical Engineering, University of Calgary, Canada, in 1996 and 2003. He is the Founding Director of the Laboratoire de Traitement de l'Information Médicale, INSERM U1101, Telecom Bretagne—Université de Bretagne Occidentale. His research interests concern advanced medical information processing, and spatial, temporal, and functional information modeling and analysis in medical images, with applications in various medical domains including orthopedics, gastroenterology, ophthalmology, cardiology, and nuclear medicine. He has published around 160 papers and holds 9 patents.

Dr. Roux was an Associate Editor of the IEEE TRANSACTIONS ON MEDICAL IMAGING (during 1993–2000), is a member of the Editorial Board of the IEEE TRANSACTIONS ON INFORMATION TECHNOLOGY and the PROCEEDINGS OF THE IEEE and chairs the GRETSI Program Committee. He served as the President of the IEEE Engineering in Medicine and Biology Society in 2001. He is the founding Cochairman of the IEEE EMBS International Summer School, Berder Island, France. He received the IEEE EMBS Award in 2003 and the INSERM Award for basic research in 2006.